Meteor-ablated Aluminum in the Mesosphere-Lower Thermosphere

John M.C. Plane[1], Shane M. Daly[1], Wuhu Feng[1,2], Michael Gerding[3] and Juan Carlos

Gómez Martín[4]

[1]School of Chemistry, University of Leeds, United Kingdom.

[2] NCAS, University of Leeds, United Kingdom.

[3] Leibniz Institute of Atmospheric Physics, Kühlungsborn, Germany.

[4] Instituto de Astrofísica de Andalucía, CSIC, 18008, Granada, Spain

Contents of this file

Figure S1. Potential energy surface for the reaction of $AlCO_3$ and O_2, calculated at the CBS-QB3 level of theory [*Montgomery et al.*, 2000].
Figure S2. Potential energy surface for the reaction of $AlCO_3$ and H, calculated at the CBS-QB3 level of theory [*Montgomery et al.*, 2000].
Figure S3. Potential energy surface for the reaction of $AlCO_3$ and H_2O, calculated at the CBS-QB3 level of theory [*Montgomery et al.*, 2000].

Table S1. Molecular properties and heats of formation (at 0 K) of the stationary points on the $OAlO_2$ + H and H_2O potential energy surfaces. The geometries are illustrated in Figure 4a and 4b in the main paper.
Table S2. Molecular properties and heats of formation (at 0 K) of the stationary points on the $Al(OH)_2$ + H potential energy surface. The geometries are illustrated in Figure 4c in the main paper.
**Table S3.** Molecular properties and heats of formation (at 0 K) of the stationary points on the $AlCO_3$ + O_2, H and H_2O potential energy surface. The geometries are illustrated in Figures S1 – S3.
Table S4. Parameters used in RRKM fits to the kinetics of AlO^+ + N_2.
**Table S5.** Rocket-borne mass spectrometric measurements of Al^+ ions used to construct the Al^+ profile in Figure 9 (main paper): payload reference number, launch location, launch time/date, and reference.

Introduction

The Figures and Tables in the SI are all referred to individually in the main paper, so please refer to that for further information beyond that contained in the captions and footnotes.
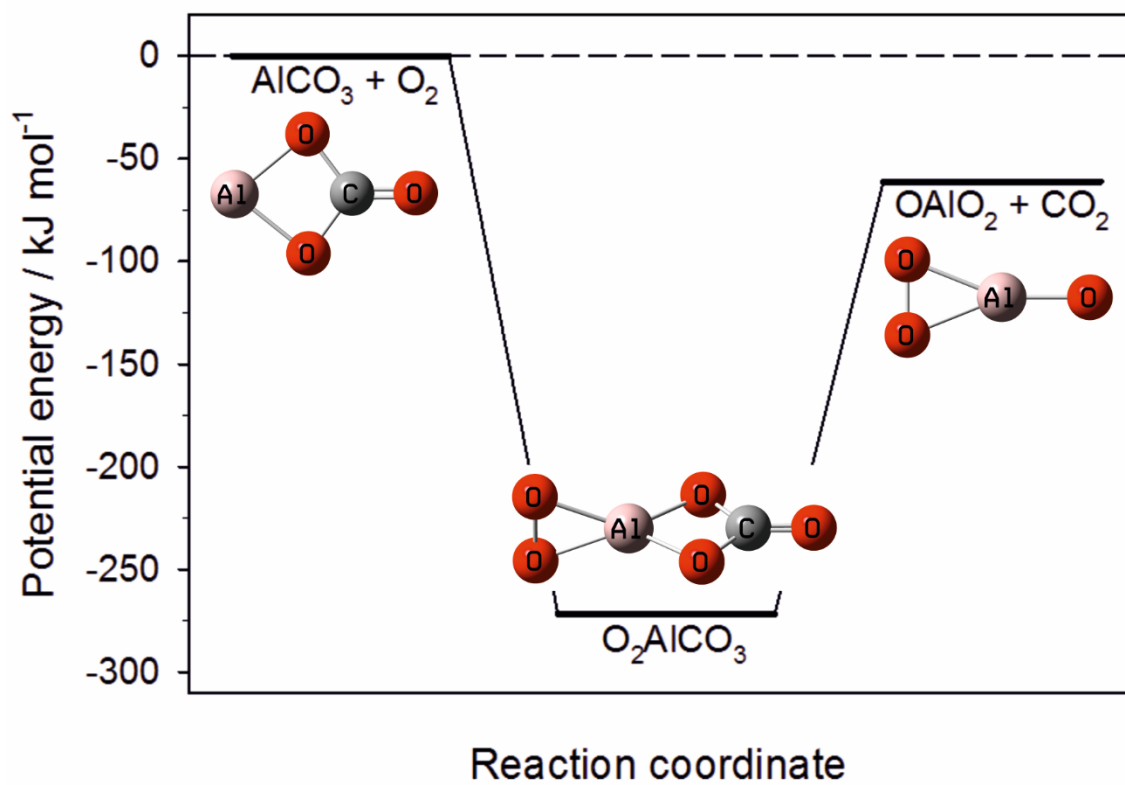
Figure S1. Potential energy surface for the reaction of $AlCO_3$ and O_2, calculated at the CBS-QB3 level of theory [*Montgomery et al.*, 2000].
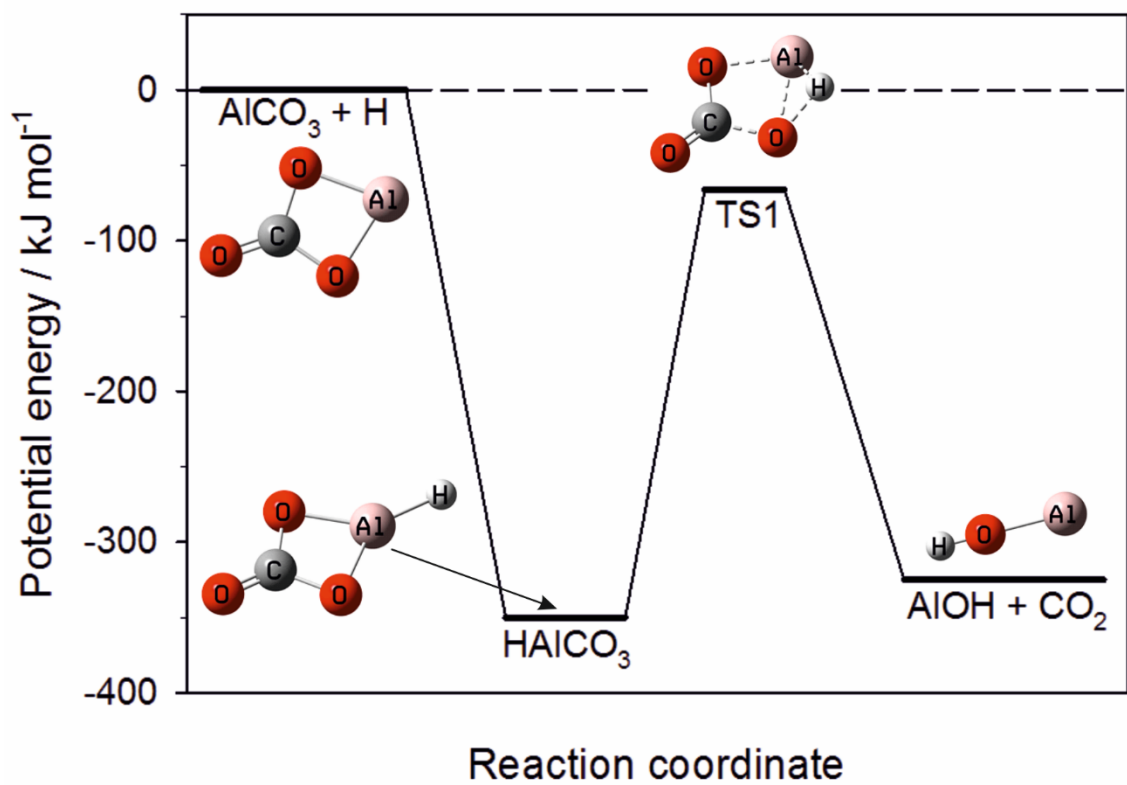
Figure S2. Potential energy surface for the reaction of $AlCO_3$ and H, calculated at the CBS-QB3 level of theory [*Montgomery et al.*, 2000].
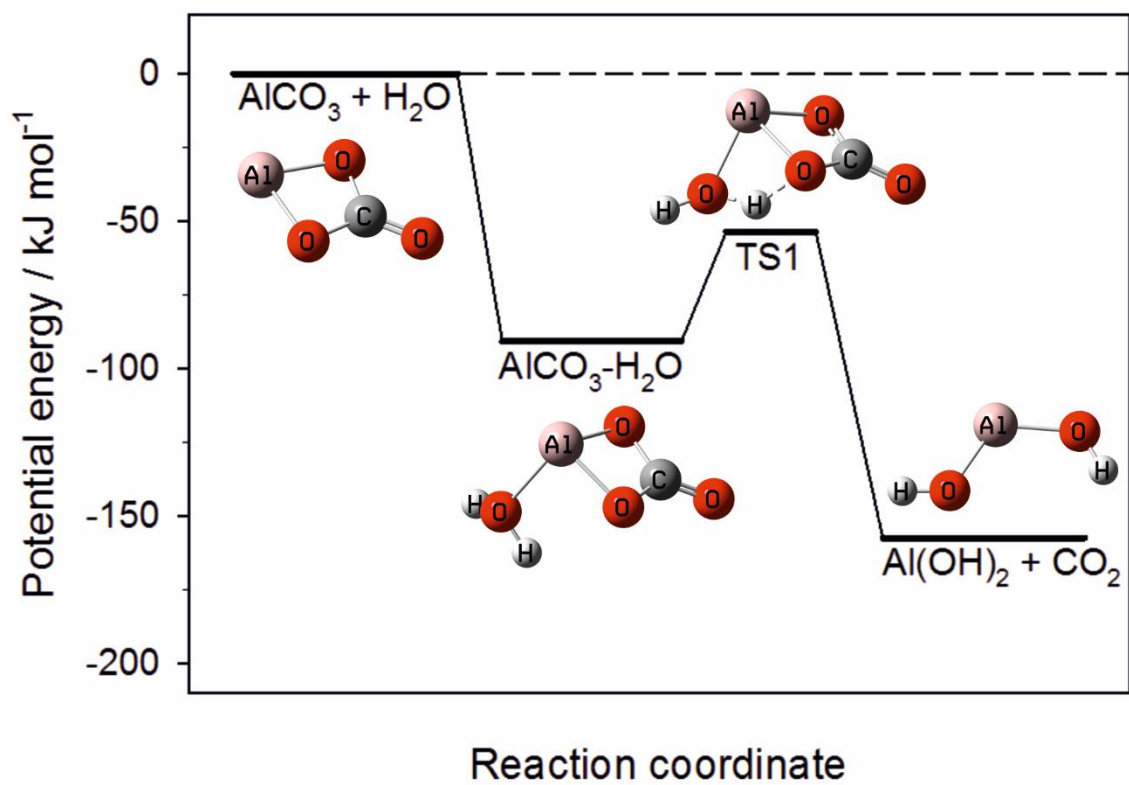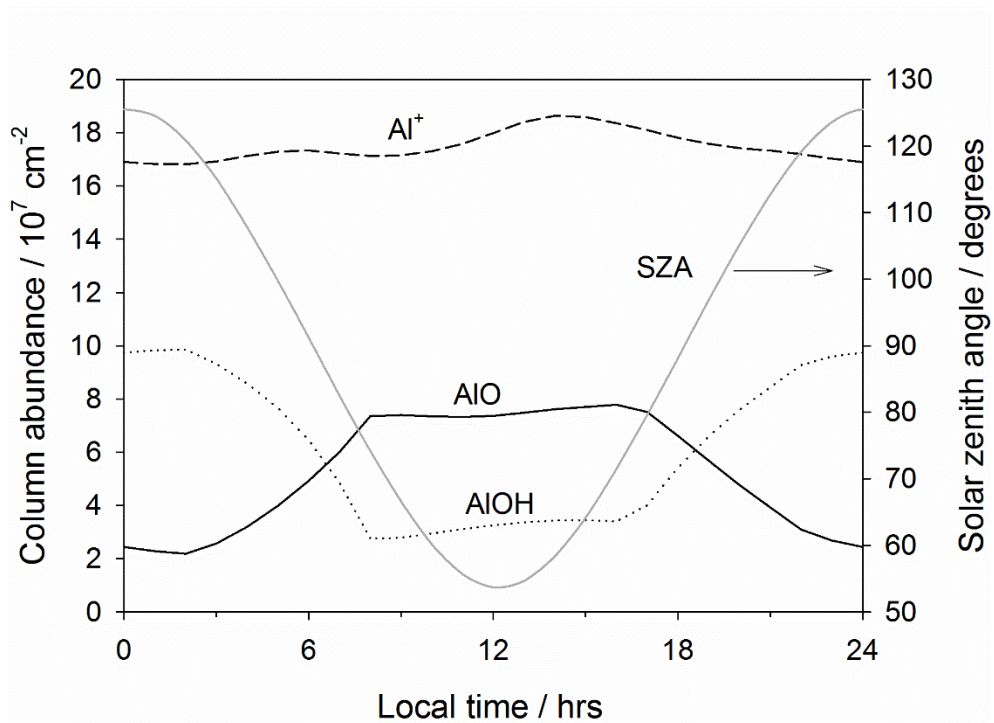
Figure S3. Potential energy surface for the reaction of $AlCO_3$ and H_2O, calculated at the CBS-QB3 level of theory [*Montgomery et al.*, 2000].

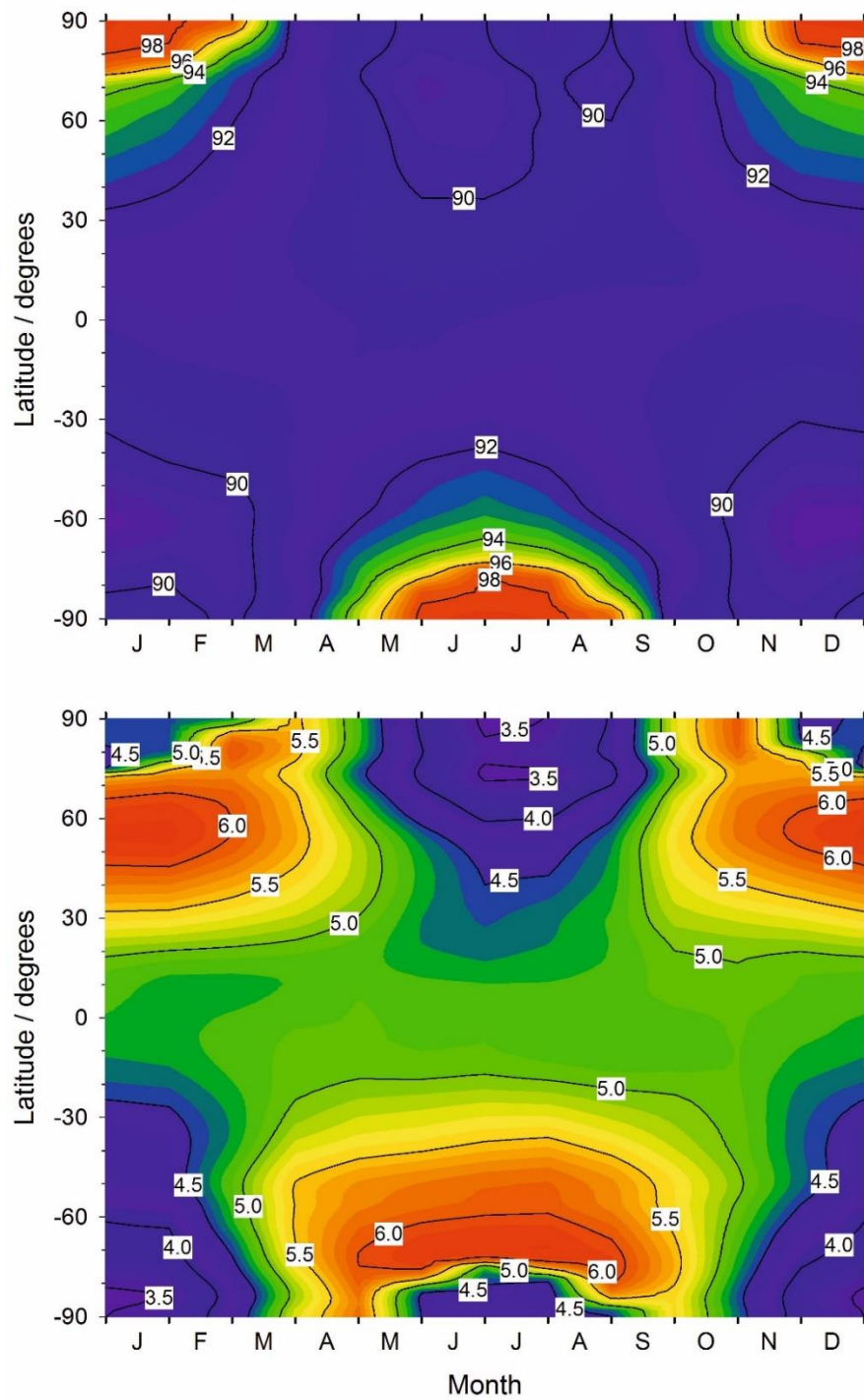**Figure S4.** Diurnal variation of the vertical column densities of AlO, AlOH and Al$^+$ at 54°N and Julian day 90. The variation of solar zenith angle is also plotted (right-hand ordinate axis).

Figure S5. Variation of the zonally-averaged AlO centroid height (upper panel, in km) and RMS width (lower panel, in km), as a function of latitude and month. Averaged data from 2004-2014.

Table S1. Molecular properties and heats of formation (at 0 K) of the stationary points on the OAlO$_2$ + H and H$_2$O potential energy surfaces. The geometries are illustrated in Figure 4a and 4b in the main paper.

Molecule (electronic state)	Geometry (Cartesian co-ordinates in Å) [a]	Rotational constants (GHz) [a]	Vibrational frequencies (cm^{-1}) [a]	$\Delta_f H^o$(0 K) (kJ mol^{-1}) [b]
OAlO$_2$ (^{2}A$_2$)	Al, 0., 0., -0.394 O, 0., -0.684, 1.318 O, 0., 0.685, 1.318 O, 0., 0., -1.994	33.702 4.0970 3.6530	189, 192, 454, 556, 1109, 1157	-148
HOAlO$_2$ (^{1}A)	Al, -0.046, -0.015, -0.284 O, -0.113, 0.049, -1.950 O, 0.071, 0.809, 1.194 O, -0.029, -0.824, 1.210 H, -0.184, -0.648, -2.603	23.110 4.3503 3.6612	205, 210, 229, 517, 570, 768, 773, 1103, 3946	-433
HOAlO$_2$ (^{3}A)	Al, 0.320, -0.595, 0.004 O, 1.744, 0.341, -0.002 O, -1.244, 0.236, 0.678 O, -1.244, 0.228, -0.680 H, 1.791, 1.300, -0.008	17.173 4.2521 4.2511	147, 202, 247, 402, 529, 613, 842, 1160, 3892	-269
AlOH (^{1}Σ)	Al, 0., 0., -0.050 O, 0., 0., 1.638 H, 0., 0., 2.592	15.492	132, 132, 819, 3982	-196
OAlO$_2$-H$_2$O	Al, -0.822, 0.809, 0.341 O, 0.693, -0.259, 0.346 O, 0.971, 0.998, -0.111 O, -2.378, 1.023, -0.041 O, -0.878, 1.544, 2.136 H, -0.339, 2.244, 2.532 H, -1.812, 1.835, 2.033	6.3241 3.4177 2.5610	71, 127, 204, 207, 307, 425, 441, 533, 553, 725, 1035, 1145, 1557, 3536, 3796	-500
TS from OAlO$_2$-H$_2$O to Al(OH)$_2$-O$_2$ (TS1)	Al, -0.182, -0.403, -0.008 O, 1.498, -0.052, 0.678 O, 1.473, 0.088, -0.681 O, -1.508, -1.343, -0.087 O, -1.306, 1.150, 0.132 H, -1.426, 1.862, -0.512 H, -1.996, 0.398, 0.008	7.0458 3.2233 2.5548	-139i, 121, 199, 209, 402, 419, 452, 560, 651 889, 1042, 33 1146, 1474, 2853, 3800	-500
Al(OH)$_2$-O$_2$	Al,0,-0.259, 0.007, 0.0 O, 0,1.46,-0.062, 0.682 O, 1.463, -0.065, -0.682	5.44625 3.96904 2.65445	148, 206, 215, 262, 288, 305,	-779

	O, -1.080, -1.470, 0.001 O, -1.083, 1.485, -0.002 H, -0.685, 2.356, 0.0126 H, -2.035, -1.554, 0.004		455, 550, 629, 636, 835, 941, 1151, 3935, 3938	
Al(OH)$_2$	Al, -0.652, 0.487, 0.110 O, 0.610, -0.630, 0.381 H, 1.148, -0.639, 1.178 O, -0.996, 1.664, 1.309 H, -1.687, 2.326, 1.234	39.607 6.5199 5.5983	214, 301, 332, 602, 620, 752, 881, 3878, 3913	-483

[a] Calculated at the B3LYP/6-311+g(2d,p) level of theory [*Frisch et al.*, 2016].

[b] Calculated at the CBS-QB3 level of theory [*Montgomery et al.*, 2000] with JANAF reference values for $\Delta_f H^o(Al) = 327.3$ kJ mol^{-1}, $\Delta_f H^o(O) = 246.8$ kJ mol^{-1}, $\Delta_f H^o(CO) = -113.8$ kJ mol^{-1}, $\Delta_f H^o(CO_2) = -393.2$ kJ mol^{-1} and $\Delta_f H^o(H_2O) = -238.9$ kJ mol^{-1} at 0 K; and $\Delta_f H^o(AlO) = 70.3$ kJ mol^{-1} [*Mangan et al.*, 2020].

Table S2. Molecular properties and heats of formation (at 0 K) of the stationary points on the $Al(OH)_2$ + H potential energy surface. The geometries are illustrated in Figure 4c in the main paper.

Molecule (electronic state)	Geometry (Cartesian co-ordinates in Å) [a]	Rotational constants (GHz) [a]	Vibrational frequencies (cm^{-1}) [a]	$\Delta_f H^o$(0 K) (kJ mol^{-1}) [b]
$Al(OH)_2$	Al, -0.652, 0.487, 0.110 O, 0.610, -0.630, 0.381 H, 1.148, -0.639, 1.178 O, -0.996, 1.664, 1.309 H, -1.687, 2.326, 1.234	39.60725 6.51988 5.59832	214, 301, 332, 602, 620, 752, 881, 3878, 3913	-483
HOAl(H)OH	Al, 0.004, -0.466, 0.252 O, 1.507, 0.309, 0.094 H, 1.615, 1.226, -0.164 O, -1.406, 0.436, -0.064 H, -2.299, 0.094, -0.007 H, -0.016, -1.971, 0.678	29.507 6.6458 5.4241	235, 348, 386, 507, 577, 635, 693, 787, 912, 2004, 3918, 3927	-624
TS from HOAl(H)OH to AlOH + H_2O	Al, -0.195, -0.843, -0.094 O, 1.363, 0.131, -0.097 H, 1.692, 0.883, 0.431 O, -1.602, 0.131, -0.061 H, -2.514, -0.166, -0.061 H, 1.460, -1.146, 0.294	30.776 6.1249 5.1493	-1482i, 182, 262, 302, 386, 544, 597, 779, 852, 1651, 3650, 3918	-328
AlOH ($^1\Sigma$)	Al, 0., 0., -0.050 O, 0., 0., 1.638 H, 0., 0., 2.592	15.49171	132, 132, 819, 3982	-196

[a] Calculated at the B3LYP/6-311+g(2d,p) level of theory [*Frisch et al.*, 2016].

[b] Calculated at the CBS-QB3 level of theory [*Montgomery et al.*, 2000] with JANAF reference values for $\Delta_f H^o$(Al) = 327.3 kJ mol^{-1}, $\Delta_f H^o$(O) = 246.8 kJ mol^{-1}, $\Delta_f H^o$(CO) = -113.8 kJ mol^{-1}, $\Delta_f H^o$(CO$_2$) = -393.2 kJ mol^{-1} and $\Delta_f H^o$(H$_2$O) = -238.9 kJ mol^{-1} at 0 K; and $\Delta_f H^o$(AlO) = 70.3 kJ mol^{-1} [*Mangan et al.*, 2020].

Table S3. Molecular properties and heats of formation (at 0 K) of the stationary points on the AlCO$_3$ + O$_2$, H and H$_2$O potential energy surface. The geometries are illustrated in Figures S1 – S3.

Molecule (electronic state)	Geometry (Cartesian co-ordinates in Å) [a]	Rotational constants (GHz) [a]	Vibrational frequencies (cm^{-1}) [a]	$\Delta_f H°(0\ K)$ (kJ mol^{-1}) [b]
AlCO$_3$ ($^3B_1$)	Al, 0.0, -1.589, 0. O, -1.111, -0.219, 0. C, -0.0, 0.605, 0. O, 0.0, 1.792, 0.0 O, 1.111,-0.219, 0.	12.789 4.1025 3.1061	189, 500, 577, 658, 794, 862, 911, 1016, 1862	-480
O$_2$AlCO$_3$	Al, 0.141, -1.466, -0.002 O, -0.947, -0.195, -0.471 C, 0.007, 0.696, 0.003 O, -0.0657, 1.878, 0.006 O, 1.065, -0.074, 0.472 O, -0.044, -3.173, 0.618 O, 0.535, -3.134, -0.622	9.2502 1.4019 1.3123	100, 112, 154, 262, 412, 500, 529, 686, 739, 793, 886, 961, 1062, 1139, 1886	-751
OAlO$_2$ ($^2A_2$)	Al, 0., 0., -0.394 O, 0., -0.684, 1.318 O, 0., 0.685, 1.318 O, 0., 0., -1.994	33.702 4.0970 3.6530	189, 192, 454, 556, 1109, 1157	-148
HAlCO$_3$	Al, 1.367, 0.0, 0.0 O, 0.014, 1.109, -0.0 C, -0.816, 0.0, 0.0 O, 0.014, -1.109, -0.0 O, -2.002, -0.0, 0.0 H, 2.917, 0.0, 0.0	12.847 3.8539 2.9646	185, 479, 496, 543, 583, 682, 800, 883, 921, 1073, 1877, 2072	-613
TS from HAlCO$_3$ to AlOH + CO$_2$	Al, 1.483, 0.089, 0.017 O, 0.013, 1.104, -0.040 C, -0.803, 0.030, -0.025 O, 0.029, -1.107, -0.162 O, -1.982, -0.002, 0.086 H, 1.086, -1.263, 0.904	11.951 3.8142 2.9373	-1346i, 158, 346, 538, 575, 601, 794, 819, 878, 1066, 1646, 1862	-330
AlOH ($^1\Sigma$)	Al, 0., 0., -0.050 O, 0., 0., 1.638 H, 0., 0., 2.592	15.49171	132, 132, 819, 3982	-196
AlCO$_3$-H$_2$O	Al, -0.620, 0.121, 1.541 O, -0.914, 0.973, -0.008 C, 0.001, 0.127, -0.591 O, 0.337, 0.132, -1.736 O, 0.464, -0.704, 0.393	6.5976 2.1681 2.0178	96, 105, 203, 218, 367, 382, 490, 544, 639, 670, 808,	-809

	O, 0.386, 1.682, 2.291 H, 0.269, 2.067, 3.170 H, 0.401, 2.391, 1.625		853, 931, 1073, 1609, 1834, 3699, 3836	
TS from $AlCO_3$-H_2O to $Al(OH)_2$ + CO_2	Al, -0.959, 0.723, 0.384 O, 0.181, -0.780, 0.729 C, 1.147, -0.121, -0.074 O, 2.226, -0.554, -0.314 O, 0.595, 1.036, -0.463 O, -1.767, -0.711, -0.502 H, -2.627, -1.116, -0.348 H, -0.794, -1.187, 0.018	6.5151 2.4560 2.0973	-1257i, 129, 200, 382, 410, 479, 534, 588, 716, 739, 806, 817, 913, 1139, 1398, 1819, 1871, 3865	-772
$Al(OH)_2$	Al, -0.652, 0.487, 0.110 O, 0.610, -0.630, 0.381 H, 1.148, -0.639, 1.178 O, -0.996, 1.664, 1.309 H, -1.687, 2.326, 1.234	39.60725 6.51988 5.59832	214, 301, 332, 602, 620, 752, 881, 3878, 3913	-483

[a] Calculated at the B3LYP/6-311+g(2d,p) level of theory [*Frisch et al.*, 2016]

[b] Calculated at the CBS-QB3 level of theory [*Montgomery et al.*, 2000], with JANAF reference values for $\Delta_f H^o(Al)$ = 327.3 kJ mol^{-1}, $\Delta_f H^o(O)$ = 246.8 kJ mol^{-1}, $\Delta_f H^o(CO)$ = -113.8 kJ mol^{-1}, $\Delta_f H^o(CO_2)$ = -393.2 kJ mol^{-1} and $\Delta_f H^o(H_2O)$ = -238.9 kJ mol^{-1} at 0 K; and $\Delta_f H^o(AlO)$ = 70.3 kJ mol^{-1} [*Mangan et al.*, 2020].

Table S4. Parameters used in RRKM fits to the kinetics of $AlO^+ + N_2 (+ N_2)$

AlO^+	Rotational constant = 16.724 GHz
	Vibrational frequency = 787 cm^{-1} [a]
N_2	Rotational constant = 60.730 GHz
	Vibrational frequency = 2447 cm^{-1} [a]
$AlO^+.N_2$	Rotational constant = 2.4664 GHz
	Vibrational frequencies: 49 ($\times$2); 228 ($\times$2); 304; 1098; 2424 cm^{-1}
$\langle \Delta E \rangle_{down} = 330 \ (T / 300)^{0.0}$ cm^{-1}	
$Z(AlO^+.N_2 + N_2) = 5.3 \times 10^{-10}$ cm^3 molecule^{-1} s^{-1} [b]; $k_\infty = 7.5 \times 10^{-10}$ cm^3 molecule^{-1} s^{-1} [c]	

[a] Calculated at the B3LYP/6-311+g(2d,p) level of theory [*Frisch et al.*, 2016]

[b] Collision frequency between the adduct and N_2

[c] High pressure limiting recombination rate coefficient, calculated from Langevin theory.

Table S5. Rocket-borne mass spectrometric measurements of Al^+ ions used to construct the Al^+ profile in Figure 9 (main paper): payload reference number, launch location, launch time/date, and reference.

Payload reference	Location	Time/date	Reference
18.1006	Wallops Islands (37.8° N, USA)	12-Aug-1976 11:58 LT	*Meister et al.* [1978]
18.1008	Wallops Islands (37.8° N, USA)	01-Jan-1977 14:03 LT	*Meister et al.* [1978]
S26/1	Kiruna (67.8° N, Sweden)	30-Jul-1978 01:32 LT	*Kopp et al.* [1985b]
S26/2	Kiruna (67.8° N, Sweden)	13-Aug-1978 01:38 LT	*Kopp et al.* [1985b]
33.010	Kiruna (67.8° N, Sweden)	16-Nov-1980 05:50 LT	*Kopp et al.* [1985a]
S37/P	Kiruna (67.8° N, Sweden)	03-Aug-1982 01:32 LT	*Kopp et al.* [1984]
18.1020	Red Lake (50.9° N, Canada)	24-Feb-1979 10:52 LT	[*Kopp*, 1997]
18.021	Red Lake (50.9° N, Canada)	26-Feb-1979 11:55 LT	[*Kopp*, 1997]

Frisch, M. J., G. W. Trucks, H. B. Schlegel, G. E. Scuseria, M. A. Robb, J. R. Cheeseman, G. Scalmani, V. Barone, G. A. Petersson, H. Nakatsuji, et al. (2016), Gaussian 16, Revision B.01, edited, Gaussian, Inc., Wallingford, CT, USA.

Kopp, E. (1997), On the abundance of metal ions in the lower ionosphere, *J. Geophys. Res.-Space Phys.*, *102*, 9667-9674.

Kopp, E., L. André, and L. G. Smith (1985a), Positive ion composition and derived particle heating in the lower auroral ionosphere, *J. Atmos. Sol. Terr. Phys.*, *47*, 301-308.

Kopp, E., P. Eberhardt, U. Herrmann, and L. G. Björn (1985b), Positive ion composition of the high-latitude summer D region with noctilucent clouds, *J. Geophys. Res.-Atmos.*, *90*, 13041-13053.

Kopp, E., H. Ramseyer, and L. G. Björn (1984), Positive ion composition and electron density in a combined auroral and NLC event, *Adv. Space Res.*, *4*, 157-161.

Mangan, T. P., J. M. Harman-Thomas, R. E. Lade, K. M. Douglas, and J. M. C. Plane (2020), Kinetic study of the reactions of AlO and OAlO relevant to planetary mesospheres, *ACS Earth Space Chem.*, *under review*.

Meister, J., P. Eberhardt, U. Herrmann, E. Kopp, M. A. Hidalgo, and J. Sechrist, CF. (1978), D-region ion composition during the winter anomaly campaign on January 8, 1977., *Space Res. XVIII*, 155-159.

Montgomery, J. A., M. J. Frisch, J. W. Ochterski, and G. A. Petersson (2000), A Complete Basis Set Model Chemistry. VII. Use of the Minimum Population Localization Method, *J. Chem. Phys.*, *112*, 6532-6542.